RSC Advances

RSC Publishing

PAPER

Dielectric behavior, band gap, *in situ* X-ray diffraction, Raman and infrared study on $(1 - x)BiVO_4$–$x(Li_{0.5}Bi_{0.5})MoO_4$ solid solution

Cite this: *RSC Advances*, 2013, **3**, 5009

Di Zhou,*[a] Li-Xia Pang,[b] Wei-Guo Qu,[c] Clive A. Randall,[d] Jing Guo,[a] Ze-Ming Qi,[d] Tao Shao[c] and Xi Yao[a]

Received 23rd October 2012,
Accepted 5th February 2013

DOI: 10.1039/c3ra22604b

www.rsc.org/advances

The phase transition in the $(1 - x)BiVO_4$–$x(Li_{0.5}Bi_{0.5})MoO_4$ solid solution was first confirmed by the *in situ* X-ray diffraction method. The merging of the (2 0 0) and (0 2 0) diffraction peaks in the X-ray diffraction data, and the overlapping of the $\delta_s(VO_4)$ and $\delta_{as}(VO_4)$ modes for Raman and Infrared spectra of $x = 0.06$ sample were observed at 110–115 °C. The splitting of infrared bands at around 325 cm^{-1} for $x = 0.125$ sample was revealed at −10 °C. The dielectric permittivity peaks as a function of temperature can be observed at high frequencies (>10 kHz), which is corresponding to the ferroelastic phase transition. In the monoclinic solid solution region, the band gaps were found to lie between 2.2–2.35 eV a range of interest as photo-catalytic materials.

I. Introduction

Recently $BiVO_4$ material has attracted attention for its ferroelasticity, dielectricity at high frequency, ion conductivity and photocatalytic properties,[1–6] which might make it useful for wide applications in gas sensors, microwave resonator devices, wastewater treatment, and water splitting. These properties strongly depend on its crystal structure. The natural $BiVO_4$ mineral crystallizes in an orthorhombic structure (with space group *Pnca*) taking on a brown color and this form has not been prepared by normal laboratory routes of ceramic synthesis such as precipitation or solid state reaction methods.[5,7] The experimentally synthesized $BiVO_4$ usually has three different structures, namely the zircon tetragonal structure (light yellow color with space group $I4_1/amd$), the scheelite monoclinic structure (yellow color with space group $I4_1/a$) and tetragonal structure (yellow color with space group $I2/a$).[5] It is known that both the orthorhombic and zircon tetragonal phases irreversibly transform to the scheelite monoclinic phase at about 400–500 °C.[7] The scheelite monoclinic phase reversibly transforms to the scheelite tetragonal phase at about 255 °C, which has been noted to be a second order ferroelastic phase transition.[8,9] The $BiVO_4$ material can be synthesized from a variety of approaches including solid state reaction method, aqueous solution precipitation method, and hydrothermal method.[10–12] The crystal structure, particle shape and size are dependent on the processing conditions.

The scheelite monoclinic $BiVO_4$ powder showed high activity for photocatalytic O_2 evolution under visible-light irradiation, while the photocatalytic activity of zircon the tetragonal and scheelite tetragonal $BiVO_4$ are small in comparison.[6,13] Furthermore, the monoclinic $BiVO_4$ was reported to possess high performance microwave dielectric properties with $\varepsilon_r = 68$, and a $Qf = 6500$–8000 GHz, $\sim TCF = -243$–-260 ppm °C^{-1}, and can be sintered temperature below 900 °C,[14,15] which indicates that it might also be a dielectric for embedded passives in low temperature co-fired ceramics (LTCC) technology. Recently, we considered compositional modifications to this basic material[16,17] with acceptor donor co-doping such as $(Li_{0.5}Bi_{0.5})^{2+}$ complex ions and Mo^{6+} ion have been employed together to substitute for the Bi^{3+} and V^{5+} in $BiVO_4$. It was found that the phase transition temperature from scheelite monoclinic to tetragonal structure was dependent on the substitution content and can be modified to become below room temperature. To study the phase transition in the $(1 - x)BiVO_4$–$x(Li_{0.5}Bi_{0.5})MoO_4$ system in more detail, *in situ* XRD, Raman and Infrared (IR) reflectivity spectra methods were employed in the present work. The compositional dependence of band gap across the solid solution ($0.0 \leqslant x \leqslant 1.0$) was also investigated.

[a]*Electronic Materials Research Laboratory, Key Laboratory of the Ministry of Education & International Center for Dielectric Research, Xi'an Jiaotong University, Xi'an, 710049, Shaanxi, P. R. China. E-mail: zhoudi1220@gmail.com; Fax: +86-29-82668794; Tel: +86-29-82668679*

[b]*Micro-optoelectronic Systems Laboratories, Xi'an Technological University, Xi'an, 710032, Shaanxi, P. R. China*

[c]*The Pennsylvania State University, Center for Dielectric Studies, Materials Research Institute, University Park, PA, 16802, USA*

[d]*National Synchrotron Radiation Laboratory, University of Science and Technology of China, Hefei, Anhui, 230029, P. R. China*

II. Experimental

The ceramic samples were prepared *via* the solid state reaction method as reported in our previous work.[16] The *in situ* XRD was performed in the temperature range from room temperature to 250 °C using a XRD with Cu-Kα radiation (XRD-7000, Shimadzu, Kyoto, Japan). Prior to examination the sintered pellets were crushed in a mortar and pestle to powder. Diffraction patterns were obtained between 15–65° 2θ at a step size of 0.02°. To obtain the dielectric characteristics at low frequencies, the monolithic ceramic samples supplied with Au electrodes were measured in the frequency range 100 Hz–1 MHz using HP 4284 device. The *in situ* Raman spectra were measured using Raman spectrometer (LabRAM HR800, HORIBA Jobin Yvon, France). The room temperature and *in situ* IR reflectivity spectra were measured using a Bruker IFS 66v FTIR spectrometer on Infrared beamline station (U4) at National Synchrotron Radiation Lab. (NSRL), China. Linear optical absorption spectra were measured by JASCO V-570 UV-Vis spectrometer at room temperature.

III. Results and discussions

Fig. 1 shows the *in situ* X-ray diffraction data, cell parameter *a* and *b* of $(1 - x)BiVO_4$–$x(Li_{0.5}Bi_{0.5})MoO_4$ sample with $x = 0.06$ recorded in the temperature range 25–250 °C. It is seen that the crystal structure continuously changed from the monoclinic to tetragonal structure as the temperature increased from 25 °C to around 110 °C, along with the characteristic merging of (2 0 0) and (0 2 0) peaks into one. This is direct evidence for the ferroelastic phase transition in $(1 - x)BiVO_4$–$x(Li_{0.5}Bi_{0.5})MoO_4$ system. As seen from Fig. 1 (b), during the phase transition the cell parameter *a* decreased while *b* increased and these became equal to each other about 5.128 Å at a temperature 110 °C, which means the tetragonal phase formation. When the temperature is increased further, the cell parameter *a* (=*b*) increased almost linearly and is consistent with thermal expansion, which is also similar to the results of pure tetragonal scheelite $BiVO_4$ materials measured above 255 °C by David and Wood.[9]

The dielectric permittivity at frequencies 100 Hz, 1 kHz, 10 kHz, 100 kHz, 1 MHz and microwave region of $x = 0.0$, $x = 0.098$ and $x = 0.10$ samples as a function of temperature (70 °C–350 °C for $x = 0.0$ sample, −50 °C–180 °C for $x = 0.098$ sample and −100 °C–160 °C for $x = 0.10$ sample) are shown in Fig. 2. The temperature dependence of the permittivity of $BiVO_4$ was first reported by Dudnik *et al.*[18] in single crystals prepared by the spontaneous crystallization from the melt. However, only an inflection at about 230 °C in the temperature dependence of permittivity was found at frequency 1.5 MHz and up to 10 MHz, which was caused by the ferroelastic phase transition. According to the classic Lyddane–Sachs–Teller relation,[19] softening of a transverse optical mode increases the relative permittivity. Hence, a maximum value of relative permittivity as a function of temperature should be observed in $BiVO_4$ sample at the ferroelastic phase transition temperature. As shown in Fig. 2(a), the permittivity increased sharply with the temperature at low frequencies 100 Hz and 1 kHz when temperature was above 100 °C. When the frequency increased to 10 kHz, an inflection could be observed at around 255 °C, which agrees with Dudnik *et al.*'s report.[18] With the further increase of frequency to 100 kHz and 1 MHz, the permittivity peaks *versus* temperature could be observed clearly due to the relative stable permittivity at high temperatures (above the phase transition temperature). As it was shown in our previous report,[17] the phase transition temperature could be lowered to around room temperature when the substitution amount of $(Li_{0.5}Bi_{0.5})MoO_4$ increased to 9.8 mol%. As seen from Fig. 2 (b) and (c), the permittivity peaks were observed only at high frequency 1 MHz and the phase transition temperature was around 50 °C for $x = 0.098$ and $x = 0.10$ samples, which is in accordance with the result at microwave region. The dielectric permittivity and dielectric loss of $x = 0.0$, $x = 0.098$, and $x = 0.10$ samples as a function of frequency (100 Hz–1 MHz) are presented in Fig. 2 (d). It is seen that all the dielectric permittivity decreased with the frequency and this might be caused by the conduction or relaxation at

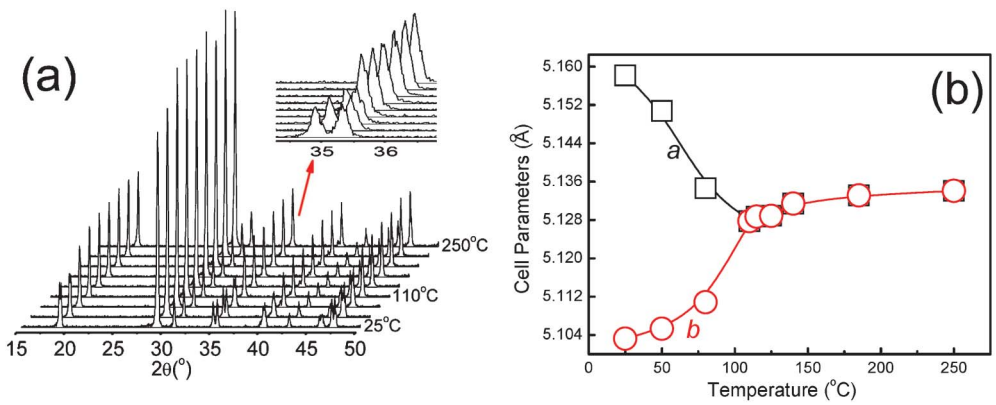

Fig. 1 *In situ* XRD data (a) and cell parameters (b) of $(1 - x)BiVO_4$–$x(Li_{0.5}Bi_{0.5})MoO_4$ ($x = 0.06$) sample in the temperature range 25–250 °C.

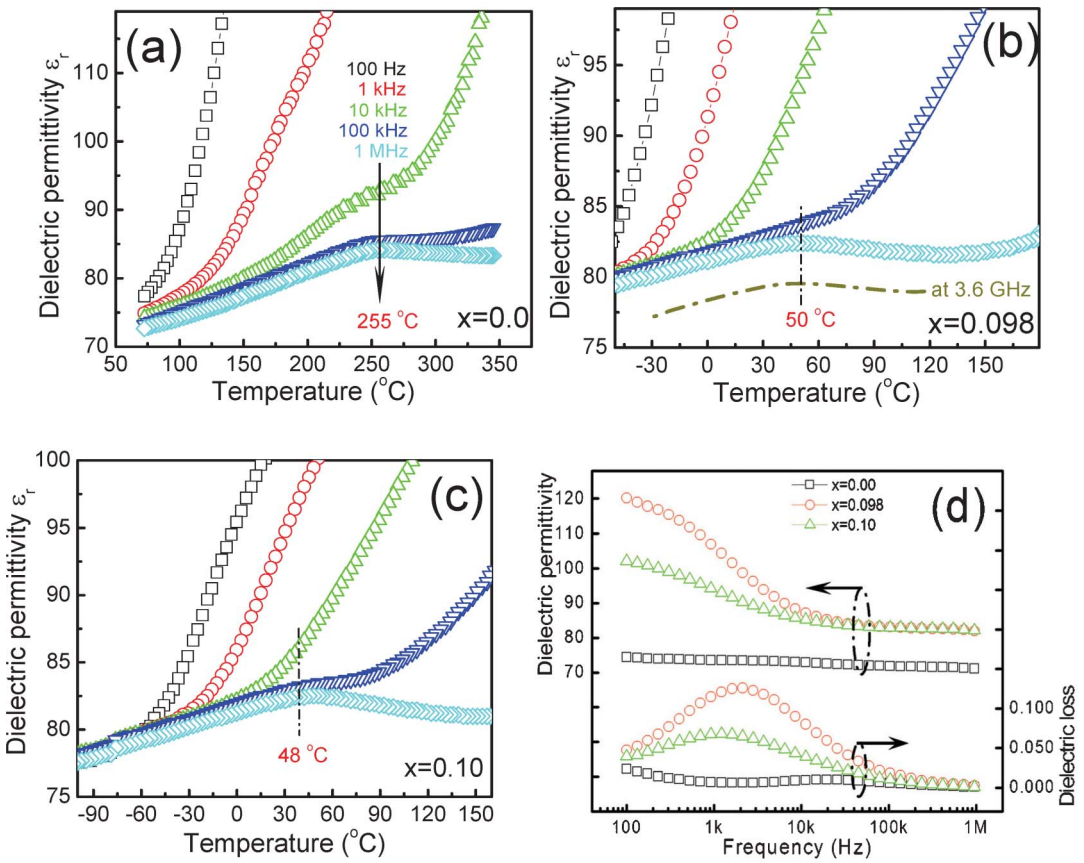

Fig. 2 Dielectric permittivity and dielectric loss at frequencies 100 Hz, 1 kHz, 10 kHz, 100 kHz, 1 MHz and microwave region of $x = 0.0$ (a), $x = 0.098$ (b), and $x = 0.10$ (c) as a function of temperature (data at 3.6 GHz for $x = 0.098$ sample from ref. 21), and as a function of frequency (d) (100 Hz–1 MHz).

low frequency, which resulted in the covering of ferroelastic phase transition peak of permittivity at low frequencies.

The *in situ* Raman spectra of $(1 - x)BiVO_4$–$x(Li_{0.5}Bi_{0.5})MoO_4$ ($x = 0.06$) sample in the temperature range 27–160 °C are presented in Fig. 3. In the spectrum recorded at 27 °C, the strongest band near 812.1 cm^{-1} is assigned to $\nu_s(VO_4)$ (Ag), and a weak shoulder at about 716 cm^{-1} is assigned to $\nu_{as}(VO_4)$ (B_g). The weak mode at around 867.5 cm^{-1} is assigned to $\nu_s(MoO_4)$ and the band for $\nu_{as}(MoO_4)$ might be covered by $\nu_s(VO_4)$ mode near 812.1 cm^{-1}. The $\delta_s(VO_4)$ (B_g) and $\delta_{as}(VO_4)$ (Ag) modes are near 357.2 and 327.4 cm^{-1}, respectively, and external modes (rotation/translation) occur near 203.7 cm^{-1} and 115.3 cm^{-1}, respectively. The weak band at 374.7 cm^{-1} is assigned to the bending mode of molybdenum anion $\delta(MoO_4)$. All the assignments correspond well with the literature results.[17,20–22] It is seen that with the increase of temperature, all the Raman peaks broaden due to increase of the average bond length and widening of the distribution of average bonds length and angles, which reflects the increase of the degree of disordering of the crystal structure. The strongest band slightly red-shifted from 812.1 cm^{-1} at 27 °C to 806.2 cm^{-1} at 160 °C and this might be caused by the bond expansion and weakening. The remarkable difference of the Raman spectra at different temperatures is the merging of the $\delta_s(VO_4)$ and

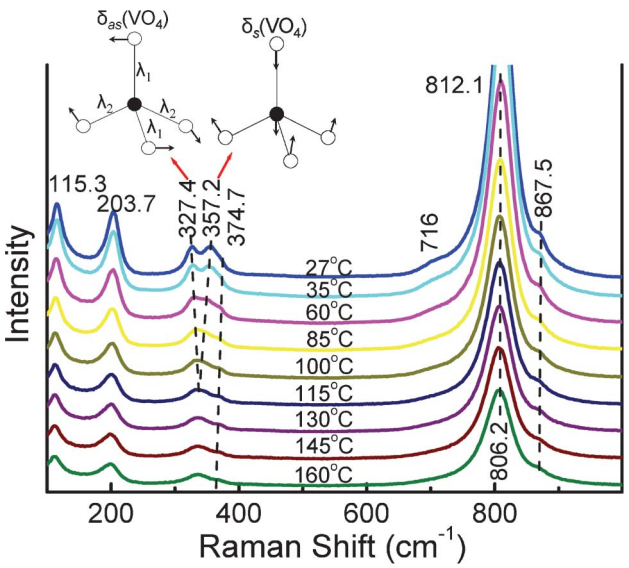

Fig. 3 *In situ* Raman spectra of $(1 - x)BiVO_4$–$x(Li_{0.5}Bi_{0.5})MoO_4$ ($x = 0.06$) sample in the temperature range 27–160 °C.

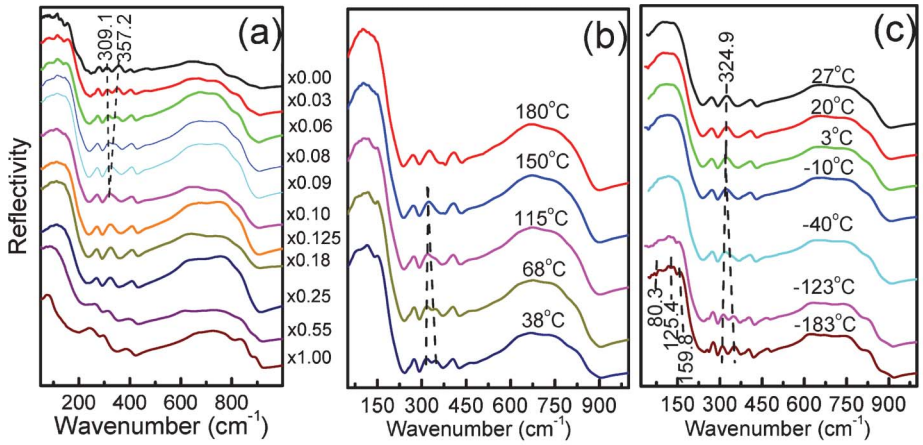

Fig. 4 Room temperature infrared spectra of $(1 - x)BiVO_4$–$x(Li_{0.5}Bi_{0.5})MoO_4$ ($0.0 \leqslant x \leqslant 1.0$) ceramics (a) and *in situ* infrared spectra of $x = 0.06$ sample (b) and $x = 0.125$ sample (c) in the temperature range −183–+180 °C.

$\delta_{as}(VO_4)$ modes at 357.2 and 327.4 cm^{-1}, respectively. As the temperature increased from 27 °C to about 115 °C, the different length λ_1 and λ_2 of V–O bonds came closer and finally became equal to each other and this results in the overlapping of $\delta_s(VO_4)$ and $\delta_{as}(VO_4)$ modes.

The room temperature infrared (IR) spectra of $(1 - x)BiVO_4$–$x(Li_{0.5}Bi_{0.5})MoO_4$ ($0.0 \leqslant x \leqslant 1.0$) ceramics are shown in Fig. 4(a). With the x value increased, it can be seen that the two bands at 309.1 cm^{-1} and 357.2 cm^{-1}, which are assigned to $\delta_{as}(VO_4)$ mode and the $\delta_s(VO_4)$ respectively, moved closer to each other and finally merged into one band at around $x = 0.10$. This is similar to the Raman analysis above and also supports the compositional phase transition at room temperature. In pure $BiVO_4$ sample, at least four sharp IR modes are observed in the range <200 cm^{-1}. These sharp IR peaks gradually overlapped as the x value increased and cannot be distinguished from each other. This might be caused by the continuous structural change from the monoclinic to the tetragonal scheelite phase. The *in situ* infrared spectra of $x = 0.06$ and $x = 0.125$ samples in the temperature range +38–+180 °C and −183–+27 °C, respectively, is shown in Fig. 4(b) and (c). The $x = 0.125$ sample belong to tetragonal phase at room temperature and there are only four IR peaks observed in the range below 450 cm^{-1}. In crystals the phase transition happens at definite temperature. Respectively, the sharp splitting should be observed in IR spectra at the transition temperature. In Fig. 4c, the transition is detected sharply at −10 °C. Meanwhile, for $x = 0.06$ sample there are at least three peaks that can be observed and separated from each other in the range below 200 cm^{-1}. The phase transition temperature of $x = 0.06$ sample were determined to be around 110 °C from *in situ* XRD analysis as discussed above. From the *in situ* infrared spectra the merging of the $\delta_{as}(VO_4)$ and the $\delta_s(VO_4)$ modes can be observed at about 115 °C. All the results can be related to the monoclinic-tetragonal scheelite phase transition.

The optical absorption property of a semiconductor, which is relevant to the electronic structure feature, is recognized as the key factor in determining its photocatalytic activity.[23,24] As x value increases, the color of samples becomes lighter and lighter from vivid-yellow for pure $BiVO_4$ to the pale-yellow for pure $(Li_{0.5}Bi_{0.5})MoO_4$. The UV-vis diffuse reflectance spectra of $(1 - x)BiVO_4$–$x(Li_{0.5}Bi_{0.5})MoO_4$ samples are shown in Fig. 5(a). All the samples ($x \leqslant 0.25$) show strong absorption in visible light region in addition to that in the UV light region. The band gap absorption edge of pure $BiVO_4$ lies between 500–550 nm, which is similar to the literature's reports. With the increase of x value, the band gap absorption edge of $(1 - x)BiVO_4$–$x(Li_{0.5}Bi_{0.5})MoO_4$ ($x \leqslant 0.25$) samples have a red-shift to between 550–600 nm. As a crystalline semiconductor, the optical absorption near the band edge follows the formula:[25]

$$\alpha h\nu = A(h\nu - E_g) \quad (1)$$

where the α, ν, E_g and A are absorption coefficient, light frequency, band gap energy and a constant, respectively. The energy of the band gap could be thus obtained from the plots of $(\alpha h\nu)^2$ *versus* photo energy ($h\nu$). The calculated band gap energies of $(1 - x)BiVO_4$–$x(Li_{0.5}Bi_{0.5})MoO_4$ as a function of x value are shown in Fig. 5(b). The band gap energy of pure $BiVO_4$ was 2.35eV, which is similar to the reported value, and the other end member $(Li_{0.5}Bi_{0.5})MoO_4$'s band gap energy was first reported here with a value about 2.87 eV, which is slightly smaller than the values of 3.1 eV for $(Na_{0.5}Bi_{0.5})MoO_4$ and 3.0 eV for $(Ag_{0.5}Bi_{0.5})MoO_4$ with the same scheelite tetragonal structure.[26] For the whole $(1 - x)BiVO_4$–$x(Li_{0.5}Bi_{0.5})MoO_4$ ($0.0 \leqslant x \leqslant 1.0$) system, the band gap energy is not proportional to composition, but reached a minimum value about 2.2 eV in the range $0.06 \leqslant x \leqslant 0.25$. In fact for most of the systems, the band gap variation with composition deviates from linearity but in a nonlinear manner, the so-called bowing effect, which can be described in by a second order equation as following:[27,28]

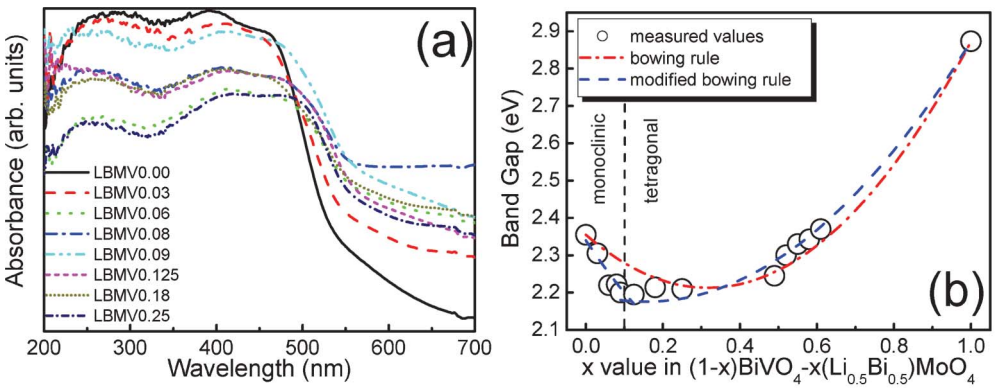

Fig. 5 UV-Vis diffuse reflectance spectra ($x \leqslant 0.25$) (a) and band gap energy variation as a function of x value (b) in $(1 - x)BiVO_4$–$x(Li_{0.5}Bi_{0.5})MoO_4$ solid solution ceramics.

$$E_g(x) = E_g(A) + (1 - x)E_g(B) - bx(1 - x) \quad (2)$$

where: $E_g(A)$ and $E_g(B)$ correspond to the band gap of the end member A and B, respectively. The parameter b is the optical bowing parameter, which is influenced by atomic size difference, chemical ionicity mismatch and atomic level heterogeneity and clustering *etc*.[29–31] The observed nonlinearity in band gap of $(1 - x)BiVO_4$–$x(Li_{0.5}Bi_{0.5})MoO_4$ samples are fitted to eqn (2), yielding a small value for the bowing parameter b of 1.37 eV. In fact the fitting is not as good as the situations in pure semiconductors and simple oxides systems, such as III–V alloys, ZnO–CrO *etc*.[32,33] This might be caused by the complex phase transition and cell parameter variation trend in $(1 - x)BiVO_4$–$x(Li_{0.5}Bi_{0.5})MoO_4$ system as reported in our previous work.[17] It is found that the phase changes gradually from monoclinic $BiVO_4$ type to the tetragonal $(Li_{0.5}Bi_{0.5})MoO_4$ type and the phase boundary is at around $x = 0.098$. The cell parameters and volume approximately follows the Vegard's law in both monoclinic and tetragonal solid solution regions, respectively, while the cell volume changes in a "V" shape *versus* the x value and a minimum value can be reached at the phase boundary. Hence, the bowing effect of the band gap variation was employed separately in both the monoclinic and tetragonal solid solution regions. The fitted values agree well with the measured values as shown by the dash line in Fig. 5(b). Compared with the traditional photo-catalyst material TiO_2 with band gap energy of 3.2 eV, which responds to UV light which occupies only 4% of the whole solar energy, the monoclinic $BiVO_4$ has been recently recognized as a strong photo-catalyst for water splitting and pollutant decomposing under visible light irradiation,[13] which accounts for 43% of the whole solar energy. The formation of the monoclinic solid solution in $(1 - x)BiVO_4$–$x(Li_{0.5}Bi_{0.5})MoO_4$ system with $0 < x \leqslant 0.098$ extended possible band gap to the range 2.2–2.35 eV, that can help to utilize more solar energy.[34] This system might be useful for new photo-catalyst materials.

IV. Conclusions

The ferroelastic phase transition in $(1 - x)BiVO_4$–$x(Li_{0.5}Bi_{0.5})MoO_4$ system was confirmed and studied by the *in situ* XRD, Raman and IR reflectivity spectra methods. For $x = 0.06$ sample, the merging of (2 0 0) and (0 2 0) peaks for XRD data at 110 °C, and the overlapping of the $\delta_s(VO_4)$ and $\delta_{as}(VO_4)$ modes at about 115 °C for Raman and infrared spectra both correspond to the phase transition, which is along with the recovery of the distorted VO_4 tetrahedron. The characteristic change of IR reflectivity spectra during phase transition can also be observed at about −10 °C for $x = 0.125$ sample. From the UV-vis diffuse reflectance spectra analysis, it can be concluded that the monoclinic solid solution in $(1 - x)BiVO_4$–$x(Li_{0.5}Bi_{0.5})MoO_4$ with $0 < x \leqslant 0.098$ has extended the band gap to a variable range 2.2–2.35 eV and this system might be useful as photo-catalytic materials for water splitting.

Acknowledgements

This work was supported by National Science Foundation of China (51202182, 51202178), the Fundamental Research Funds for the Central University, headmaster foundation of Xi'an Technological University (XAGDXJJ1001), and the Foundation of Shaanxi Educational Committee (12JK0432). The author would like to thank Qiu-Ping Wang, Han-Chen Liu, Chao Zhou, Jinzhan Su and Xiao-Hui Song for their help in Raman and UV experiments and the administrators in IR beamline workstation of National Synchrotron Radiation Laboratory (NSRL) for their help with the IR measurements. We also wish to thank the National Science Foundation I/UCRC program, as part of the Center for Dielectric Studies under Grant No. 0628817, for partial support and also the MCL facilities at Penn State University.

References

1 W. I. F. David and I. G. Wood, *J. Phys. C: Solid State Phys.*, 1983, **16**, 5149.

2 M. Valant and D. Suvorov, *J. Am. Ceram. Soc.*, 2000, **83**, 2721.
3 H. Wienand, W. Ostertag and K. Bittler, *US Patent*, 1984, 4455174.
4 T. H. Yeom, S. H. Choh, M. L. Du and M. S. Jang, *Phys. Rev. B: Condens. Matter*, 1996, **53**, 3415.
5 A. K. Bhattacharya, K. K. Mallick and A. Hartridge, *Mater. Lett.*, 1997, **30**, 7.
6 H. Liu, J. Yuan, Z. Jiang, W. F. Shangguan, H. Einaga and Y. Teraoka, *J. Mater. Chem.*, 2011, **21**, 16535.
7 R. S. Roth and J. L. Waring, *Am. Mineral.*, 1963, **48**, 1348.
8 J. D. Bierlein and A. W. Sleight, *Solid State Commun.*, 1975, **16**, 69.
9 W. I. F. David and I. G. Wood, *J. Phys. C: Solid State Phys.*, 1983, **16**, 5127.
10 A. R. Lim, S. H. Choh and M. S. Jang, *J. Phys.: Condens. Matter*, 1995, **7**, 7309.
11 J. L. Blin, A. Lorriaux-Rubbens, F. Wallart and J. P. Wignacourt, *J. Mater. Chem.*, 1996, **6**, 385.
12 J. Q. Yu and A. Kudo, *Chem. Lett.*, 2005, **34**, 850.
13 A. Kudo, K. Ueda, H. Kato and I. Mikami, *Catal. Lett.*, 1998, **53**, 229.
14 M. Valant and D. Suvorov, *J. Am. Ceram. Soc.*, 2000, **83**, 2721.
15 S. H. Wee, D. W. Kim and S. I. Yoo, *J. Am. Ceram. Soc.*, 2004, **87**, 871.
16 D. Zhou, C. A. Randall, H. Wang, L. X. Pang and X. Yao, *J. Am. Ceram. Soc.*, 2010, **93**, 2147.
17 D. Zhou, W. G. Qu, C. A. Randall, L. X. Pang, H. Wang, X. G. Wu, J. Guo, G. Q. Zhang, L. Shui, Q. P. Wang, H. C. Liu and X. Yao, *Acta Mater.*, 2011, **59**, 1502.
18 E. F. Dudnik, V. V. Gene, S. V. Akimov and A. Y. Kreicher, *Fizika Tverdogo Tela*, 1974, **16**, 2733.
19 R. H. Lyddane, H. Sachs and E. Tellar, *Phys. Rev.*, 1941, **59**, 673.
20 R. L. Frost, D. A. Henry, M. L. Weier and W. Martens, *J. Raman Spectrosc.*, 2006, **37**, 722.
21 F. D. Hardcastle, I. E. Wachs, H. Eckert and D. A. Jefferson, *J. Solid State Chem.*, 1991, **90**, 194.
22 J. Yu and A. Kudo, *Adv. Funct. Mater.*, 2006, **16**, 2163.
23 J. Tang, Z. Zou and J. Ye, *Angew. Chem., Int. Ed.*, 2004, **43**, 4463.
24 J. Tang, Z. Zou and J. Ye, *Chem. Mater.*, 2004, **16**, 1644.
25 M. A. Butler, *J. Appl. Phys.*, 1977, **48**, 1914.
26 H. Kato, N. Matsudo and A. Kudo, *Chem. Lett.*, 2004, **33**, 1216.
27 J. E. Bernardand and A. Zunger, *Phys. Rev. B*, 1986, **34**, 5992.
28 S. Lee, W. H. Woodford and C. A. Randall, *Appl. Phys. Lett.*, 2008, **92**, 201909.
29 H. L. Shi and Y. Duan, *Eur. Phys. J. B*, 2008, **66**, 439.
30 S. Lee, R. D. Levi, W. G. Qu, S. C. Lee and C. A. Randall, *J. Appl. Phys.*, 2010, **107**, 023523.
31 I. Levin, E. Cockayne, V. Krayzman, J. C. Woicik, S. Lee S and C. A. Randall, *Phys. Rev. B: Condens. Matter Mater. Phys.*, 2011, **83**, 094122.
32 G. P. Donati, R. Kaspi and K. J. Malloy, *J. Appl. Phys.*, 2003, **94**, 5814.
33 S. Adachi, *Properties of Semiconductor Alloys: Group-IV, III-V and II-VI Semiconductors*, Wiley, New York, 2009.
34 D. Zhou, L. X. Pang, H. Wang, J. Guo, X. Yao and C. A. Randall, *J. Mater. Chem.*, 2011, **21**, 18412.